Diversity Combining via Universal Orthogonal Space-Time Transformations

Elad Domanovitz and Uri Erez

***Abstract*—Receiver diversity methods play a key role in combating the detrimental effects of fading in wireless communication and other applications. Commonly used linear diversity methods include maximal ratio combining, equal gain combining and antenna selection combining. A novel linear combining method is proposed where a universal orthogonal dimension-reducing space-time transformation is applied prior to quantization of the signals. The scheme is particularly well-suited to reduced-complexity analog-to-digital conversion of narrowband signals as well as provides a method to achieve diversity-enhanced relaying of communication signals, for multi-user detection in at a remote terminal, minimizing the required bandwidth used in the links between relays and terminal.**

I. Introduction

In wireless communication, diversity methods play a central role in combating the detrimental effects of severe channel variation (fading). Of the many techniques that have been developed over the years with this goal, an important class involves the use of multiple receive antennas. With sufficient separation between the antennas, each antenna may be viewed as a branch receiving the transmitted signal multiplied by an approximately independent fading coefficient. Diversity is achieved as the probability that the signal is severely affected by fading on all branches simultaneously is greatly reduced. The number of such (roughly) independent branches is commonly referred to as the diversity order. A classical survey of receive diversity techniques is [1]. More recent accounts that also consider multiple-input multiple-output channels are [2], [3].

We introduce a new diversity-combining scheme utilizing orthogonal space-time block codes. The key difference between the proposed scheme and traditional linear combining schemes is that it is *universal*. That is, the combining weights (in the proposed scheme, the space-time transformation) do not depend on the the channel realization.

To understand the potential benefits as well as the general nature of the contribution, consider a receiver as depicted in Figure 1. A key feature of modern device architectures is the decomposition of the unit into separate functional blocks (that can be located at different physical locations, i.e., distributed processing). These blocks are connected by interfaces and a major design goal is to reduce the bandwidth between different blocks.

The proposed scheme can assist in the interface from the analog domain to the digital one, simplifying analog-to-digital conversion (ADC) and thus also reducing power consumption. The scheme can equally assist in reducing the bandwidth of the digital interface between different digital blocks. For example, in a centralized (cloud) radio access network (C-RAN) setting, this bandwidth reduction will be in the fronthaul links between the relays (remote radio head units) and the central (cloud) processing unit.

The rest of the paper is organized as follows. In Section II we describe the scheme in the most basic setup of a single-input multiple-output (SIMO) system with only two receive antennas.

II. Description of the Scheme for Two Receive Antennas

Consider a 2×1 SIMO channel as depicted in Figure 1. The signal received at antenna $i = 1, 2$, at discrete time t is

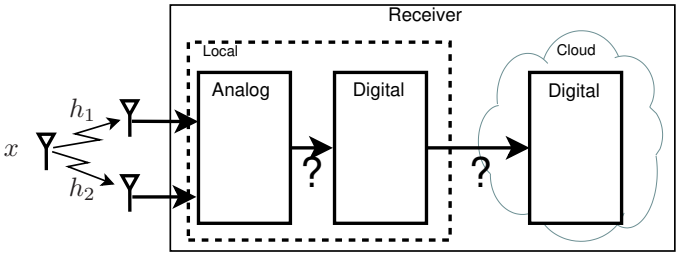

Fig. 1. Basic scenario: receiver architecture for a 2×1 SIMO channel.

given by

$$s_i(t) = h_i x(t) + n_i(t). \tag{1}$$

We assume that the noise $n_i(t)$ is i.i.d. over space and time with samples that are circularly-symmetric complex Gaussian with unit variance.

The scheme works on batches of two time instances and for our purposes, it will suffice to describe it for time instances $t = 1, 2$. Let us stack these four complex samples received over $T = 2$ time instances, two over each antenna, into an 8×1 real vector:

$$\mathbf{s} = [s_{1R}(1) s_{1I}(1) s_{2R}(1) s_{2I}(1) s_{1R}(2) s_{1I}(2) s_{2R}(2) s_{2I}(2)]^T, \tag{2}$$

where x_R and x_I denote the real and imaginary parts of a complex number x. We similarly define the stacked noise vector $\mathbf{n}$. Likewise, we define

$$\mathbf{x} = [x_R(1)\, x_I(1)\, x_R(2)\, x_I(2)]^T. \tag{3}$$

Next, we form a 4×1 real vector $\mathbf{u}$ by applying to the vector $\mathbf{s}$ the transformation

$$\mathbf{u} = P\mathbf{s}$$

where

$$P = \frac{1}{\sqrt{2}} \begin{bmatrix} 1 & 0 & 0 & 0 & 0 & 0 & 1 & 0 \\ 0 & 1 & 0 & 0 & 0 & 0 & 0 & -1 \\ 0 & 0 & 1 & 0 & -1 & 0 & 0 & 0 \\ 0 & 0 & 0 & 1 & 0 & 1 & 0 & 0 \end{bmatrix}. \quad (4)$$

Note that unlike conventional linear diversity combining schemes, here the combining matrix P does not depend on the channel coefficients. In other words, it is universal.

It is not hard to show that the following holds

$$\begin{aligned} \mathbf{u} &= U(h_1, h_2)\mathbf{x} + P\mathbf{n} \\ &= U(h_1, h_2)\mathbf{x} + \mathbf{n}', \end{aligned} \quad (5)$$

where

$$U(h_1, h_2) = \frac{1}{\sqrt{2}} \begin{bmatrix} h_{1R} & -h_{1I} & h_{2R} & -h_{2I} \\ h_{1I} & h_{1R} & -h_{2I} & -h_{2R} \\ h_{2R} & -h_{2I} & -h_{1R} & h_{1I} \\ h_{2I} & h_{2R} & h_{1I} & h_{R1} \end{bmatrix}. \quad (6)$$

A key observation is that $U(h_1, h_2)$ is an orthogonal matrix for any h_1, h_2:

$$U^H(h_1, h_2)U(h_1, h_2) = \|\mathbf{h}\|^2 \cdot I, \quad (7)$$

where I is the identity matrix. Further, since the rows of P are orthogonal, it follows that $\mathbf{n}'$ is white and Gaussian with unit variance.

We next apply to $\mathbf{s}$ (component-wise) a scalar uniform quantizer $Q(\cdot)$ to obtain

$$\mathbf{y} = \begin{bmatrix} y_1(t=1) \\ y_2(t=1) \\ y_1(t=2) \\ y_2(t=2) \end{bmatrix} = Q[\mathbf{u}].$$

We denote the quantization error vector by

$$\begin{aligned} \mathbf{e} &= \mathbf{u} - \mathbf{y} & (8) \\ &= \mathbf{u} - Q(\mathbf{u}). & (9) \end{aligned}$$

The sequence of quantized samples is used to reconstruct an estimation of the source vector

$$\hat{\mathbf{x}} = \begin{bmatrix} \widehat{x_R(t=1)} \\ x_I(t=1) \\ x_R(t=2) \\ x_I(t=2) \end{bmatrix} \quad (10)$$

by applying the transformation:

$$\hat{\mathbf{x}} = \frac{1}{\|\mathbf{h}\|} U(h_1, h_2)^H \mathbf{y}. \quad (11)$$

Using (5) and (9), we have

$$\begin{aligned} \hat{\mathbf{x}} &= \frac{1}{\|\mathbf{h}\|} U(h_1, h_2)^H (\mathbf{u} - \mathbf{e}) & (12) \\ &= \frac{1}{\|\mathbf{h}\|} U(h_1, h_2)^H (U(h_1, h_2)\mathbf{x} + \mathbf{n}' - \mathbf{e}) & (13) \\ &= \frac{\|\mathbf{h}\|}{\sqrt{2}} \mathbf{x} + \mathbf{n}'' - \mathbf{e}', & (14) \end{aligned}$$

where $\mathbf{n}''$ has the same distribution as $\mathbf{n}$.

As for the quantization error $\mathbf{e}$ and its transformed variant $\mathbf{e}'$, we may invoke the standard assumption, which may be justified using subtractive dithered quantization, that it is independent of the signal (and hence of $\mathbf{x}$) and is white (i.e., its covariance matrix is the identity).

We conclude that the input/output relationship of the proposed diversity combiner is identical to that of MRC, except for a power loss of a factor of two. In other words, we attain full diversity but no array gain, precisely as in the case of Alamouti space-time diversity transmission.

III. Application to analog-to-digital conversion

In this section we demonstrate the effectiveness of the scheme to analog-to-digital conversion for narrowband internet-of-things power-limited devices [4]–[6].

The proposed method may be used to achieve maximal diversity order with a single radio-frequency (RF) chain and analog-to-digital converter, and without requiring a switching mechanism which comes at substantial analog hardware complexities; see discussion of hardware aspects in [3]. In this section we do not explicitly consider the quantization noise as it behaves in very much the same way in all systems considered.

Consider again the scenario of a 2×1 SIMO system as depicted in Figure 1 and described in the previous section. We note that as the fading coefficient are constants (rather than impulse responses), the model assumed is that of frequency-flat fading.

The role of diversity is easiest to understand by assuming first that the receiver front end arbitrarily processes the output of one antenna only, say, only the output of antenna 1, as depicted in Figure 2. Thus, only the signal $s_1(t)$ in (1) passes

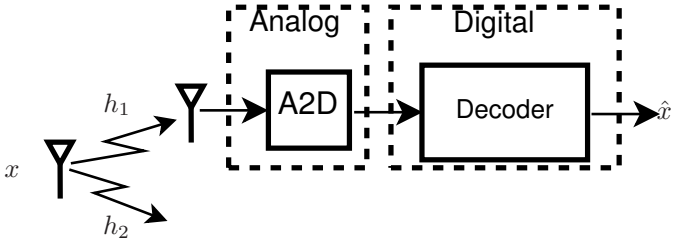

Fig. 2. Demonstration of a receiver that chooses an arbitrary branch for processing.

through the RF chain and a single A/D unit suffices. The performance however is far from robust as a fade of a single channel coefficient (h_1 with our arbitrary choice) will result in highly degraded signal-to-noise ratio (SNR). In a Rayleigh fading environment, the bit error rate for uncoded transmission will decay as

$$P_e \sim SNR^{-d} \quad (15)$$

where here $d = 1$, and we say that we have first order diversity. Similarly, in a system where $d = 2$ as will be described below, we have a diversity order of 2.

The best performance may be attained by quantizing the output of each antenna and then using maximal-ratio combining (MRC) as depicted in Figure 3. This produces an effective

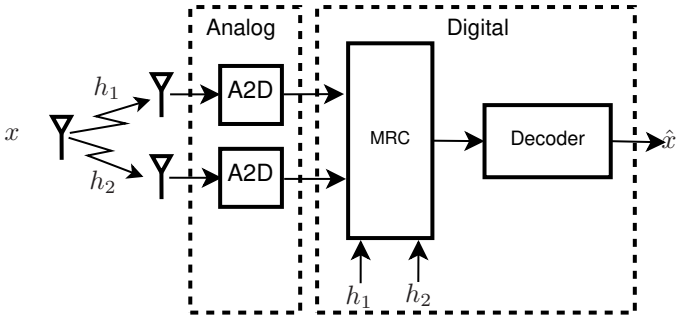

Fig. 3. A receiver employing a maximal-ratio combining front end.

scalar channel

$$y_{\mathrm{MRC}} = \|\mathbf{h}\|x + n, \tag{16}$$

As the variation of $\|\mathbf{h}\|$ is much smaller than that of either h_1 or h_2, diversity is attained. This may intuitively be understood by noticing that both h_1 and h_2 have to vanish in order for h to vanish. When h_1 and h_2 are independent, we obtain a diversity order of 2. The precise performance of MRC under independent Rayleigh fading is well-known and may be found, e.g., in [1]. The major downside of such a system is that two RF chains and A/Ds are needed.

A classic alternative to MRC that requires only one RF chain is the method of antenna selection or "selection combining" as depicted in Figure 4.

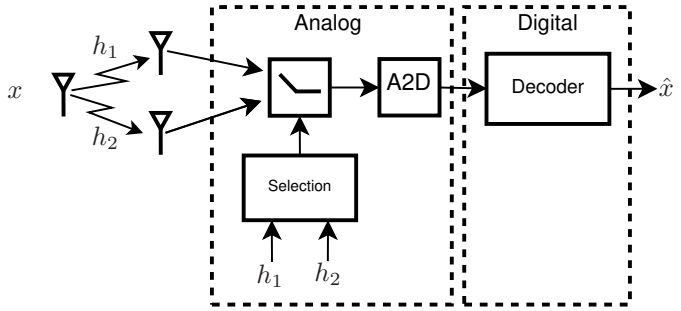

Fig. 4. A receiver employing selection-diversity combining as a front end.

Here, rather than choosing the antenna arbitrarily, we choose the one with the higher SNR. Thus the effective channel becomes

$$y_{\mathrm{SC}} = \max(|h_1|, |h_2|)x + n, \tag{17}$$

While the performance does not reach that of MRC, it does attain a diversity order of 2. Again, the precise performance under independent Rayleigh fading of selection combining is well-known and may be found, e.g., in [1]. One downside of selection combining method is that it requires analog detection and switching mechanisms.

We may use the novel space-time diversity combining method described in the previous section, as depicted in Figure 5. Now the effective channel takes the form

$$y_{\mathrm{ST}} = \frac{\|\mathbf{h}\|}{\sqrt{2}}x + n. \tag{18}$$

It follows that the scheme also attains a diversity order of 2 but loses precisely a factor of two in terms of SNR with respect to MRC. In comparison with selection combining (without taking into account implementation losses), there a loss in the achieved SNR while an advantage is that no estimation of channel quality in the analog front end nor switching is required.

A comparison of the performance of the proposed method is shown in Figure 6 which plots the bit error rate of all three methods for uncoded QPSK transmission.

IV. Application to Multi-User Detection in the Cloud

The real strength of the proposed method appears in distributed scenarios as we now exemplify in the context of 5G multi-user detection in the cloud. [7]–[10].

Unlike in the previous section, the scheme we present now operates purely in the digital domain. We assume that each antenna is sampled separately and the benefit is not in the realm of hardware simplification but rather in making efficient use of the limited bit rate available in the fronthaul link in a C-RAN setting.

A further difference is that we no longer assume frequency-flat fading. Rather, we will assume that a font-end operation after A/D conversion is to apply a DFT operation, thus working in the frequency domain. In other words, the static channel we will consider is to be understood to apply to a single tone. The "time" index t will correspondingly refer to subsequent uses of the same tone, or in a practical setting could apply to adjacent tones as these typically have very similar channel coefficients.

As a baseline system, consider the system depicted in Figure 7 in which two users wish to communicate with a base station via two relays, where both users as well as the relays are equipped with a single antenna. The relays are connected to the base station via rate-constrained bit pipes.

The latter scenario has been extensively studied and we refer the reader to [10] and references therein for background. In this section we show how the space-time diversity method developed in the present work can serve as a simple and practical means to reap a substantial part of the gains promised by the vast body of theory already established.

The received signal at relay $i = 1, 2$ is given by

$$s^i(t) = h^i_{11} \cdot x_1(t) + h^i_{12} \cdot x_2(t) + n^i_1(t), \tag{19}$$

where h^i_{jk} denotes the channel gain between user k and antenna j in relay i. Since currently we are considering single-antenna relays, $j = 1$.

We employ the most basic compress-and-forward protocol where correlation between the received signals is ignored and each relay simply quantizes the received signal and sends the quantized output via its bit pipe. To simplify the exposition and since the quantization noise will again behave in much the same manner in all schemes to be considered, we do not account for it in the system description in the sense that we assume that it is negligible with respect to the Gaussian noise (although it plays an important role in determining the rate needed to be supported by the bit pipes).

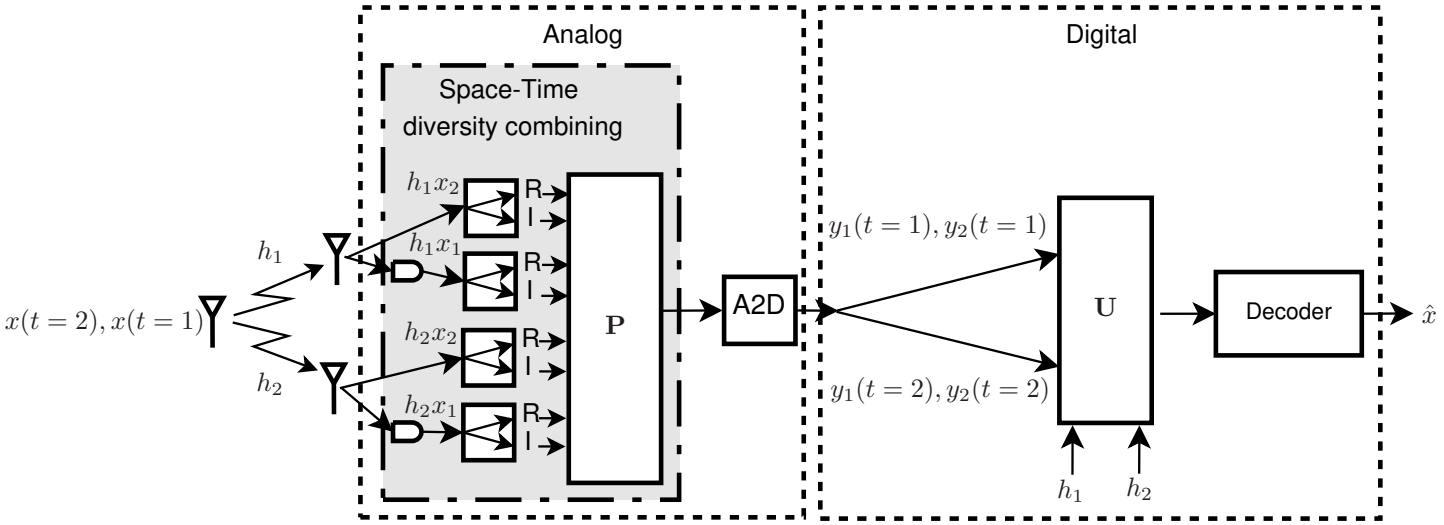

Fig. 5. Novel receiver front end employing an orthogonal space-time diversity transformation.

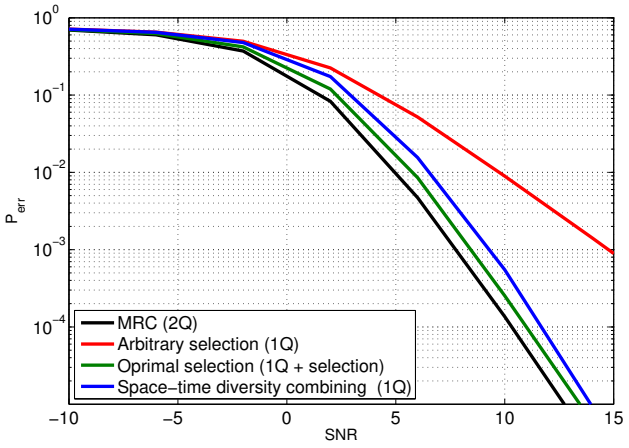

Fig. 6. Performance of bit error rate of new space-time diversity scheme and comparison with alternatives.

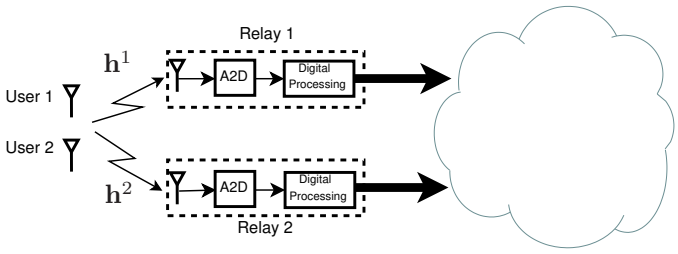

Fig. 7. Baseline uplink scenario in C-RAN: a two-user virtual MIMO system formed by two single-antenna relays connected to the cloud via rate-constrained fronthaul links.

The base station thus receives at each time instance (the time index plays no role at this point) the vector

$$\mathbf{y} = (s_1(t), s_2(t))^T.$$

We assume that it also knows (is able to estimate) the channel coefficients and thus can form the combined effective matrix

$$G = \left[\begin{array}{cc} h_{11}^1 & h_{12}^1 \\ \hline h_{11}^2 & h_{12}^2 \end{array} \right], \tag{20}$$

where the upper part of the matrix corresponds to the signal originating from relay 1 and the bottom corresponds to relay 2.

It next applies a linear equalizer to obtain a soft estimation of the source vector. For instance, it may use a zero forcing equalizer,

$$\left[\begin{array}{c} \widehat{x_1(t)} \\ x_2(t) \end{array} \right] = G^{-1}\mathbf{y}, \tag{21}$$

or a linear minimum mean square error (MMSE) equalizer. Assuming uncoded transmission for simplicity, the latter vector is then fed into a slicer.

Now consider the same scenario except that each relay is now equipped with two antennas, rather than one, as depicted in Figure 8. Thus, received signal at relay $i = 1, 2$ and antenna $j = 1, 2$ is given by

$$s_j^i(t) = h_{j1}^i \cdot x_1(t) + h_{j2}^i \cdot x_2(t) + n_j^i(t), \tag{22}$$

Thus, the channel matrix of relay i is

$$H^i = \left[\begin{array}{cc} h_{11}^i & h_{12}^i \\ h_{21}^i & h_{22}^i \end{array} \right]. \tag{23}$$

The question now arises as to how best to utilize the finite number of bits available per sample in quantizing the output of the two antennas. Due to the distributed nature of the problem, both MRC and selection combining are inapplicable as the base station is interested in recovering both signals. In other words, consider antenna selection and suppose that one user experiences a higher SNR at antenna 1 and the situation is reversed for the other user; which antenna should one select?

We now demonstrate that while keeping the bit rate fixed, each relay can nonetheless provide diversity gains to *both users* using the novel combining method, precisely since it makes no use of channel state information at the quantization

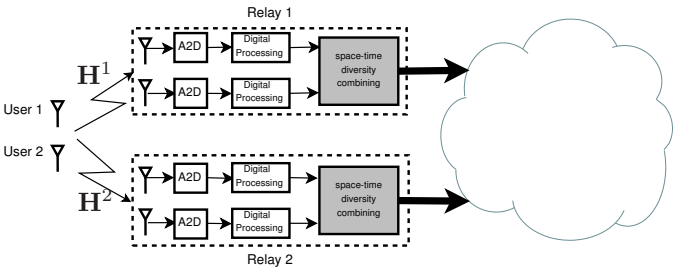

Fig. 8. Multi-antenna uplink scenario in C-RAN: two-user virtual MIMO system formed by two two-antenna relays connected to the cloud via rate-constrained fronthaul links.

stage, rather only in the reconstruction stage.

Assuming both relays use the scheme, the signal passed to the cloud from relay i is given by

$$\mathbf{u}^i = U(h^i_{11}, h^i_{21})\mathbf{x}_1 + U(h^i_{12}, h^i_{22})\mathbf{x}_2 + \mathbf{n}'^i, \qquad (24)$$

where $\mathbf{x}_j$ represents the real representation of the signal transmitted by user j over the two time instances according to the notation in (3). Thus, at the cloud we obtain the combined relation

$$\begin{bmatrix} \mathbf{u}^1 \\ \mathbf{u}^2 \end{bmatrix} = \underbrace{\left[\begin{array}{c|c} U(h^1_{11}, h^1_{12}) & U(h^1_{21}, h^1_{22}) \\ \hline U(h^2_{11}, h^2_{12}) & U(h^2_{21}, h^2_{22}) \end{array}\right]}_{\mathcal{G}} \begin{bmatrix} \mathbf{x}_1 \\ \mathbf{x}_2 \end{bmatrix} + \begin{bmatrix} \mathbf{n}'^1 \\ \mathbf{n}'^2 \end{bmatrix} \qquad (25)$$

Note that the effective matrix $\mathcal{G}$ has the desirable property that each of the four submatrices is orthogonal. Thus, it is expected that applying zero-forcing to the effective channel followed by a slicer (or in general, a decoder) will perform better than the baseline scheme.

The performance of the proposed scheme is demonstrated in Figure 9 and Figure 10. Figure 9 shows the bit error rate achieved by the scheme for uncoded QPSK transmission as well as the baseline scheme, which may be thought of as choosing one antenna at arbitrary. As another benchmark, we also plot the performance obtained for the same receiver structure (linear MMSE equalization followed by a slicer) where the central receiver obtains the output of all four antennas (two from each relay).

Figure 10 compares the three schemes with the same (linear MMSE) equalization but coupled with ideal coding over many i.i.d. realization of the channel. Specifically, we depicts the ergodic capacity associated with each combining method.

V. Discussion: Extensions to More than Two Antennas

As in the case of space-time modulation, extension to more receive antennas is possible, albeit with some loss.

A natural approach is to try utilizing the theory of orthogonal designs. It should be noted however that it is well known that the decoding delays (number of time instances stacked together) roughly grows exponentially with the number of antennas. Another possible avenue is to try to follow the approach of quasi-orthogonal space-time codes as developed in [11]–[13].

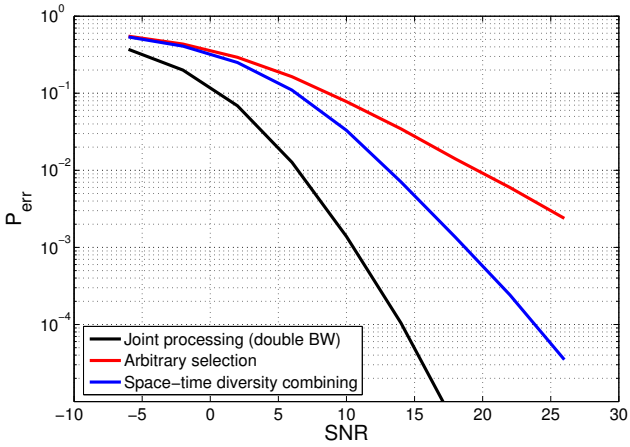

Fig. 9. Bit error rate of compress-and-forward using the proposed method with the three considered combining methods.

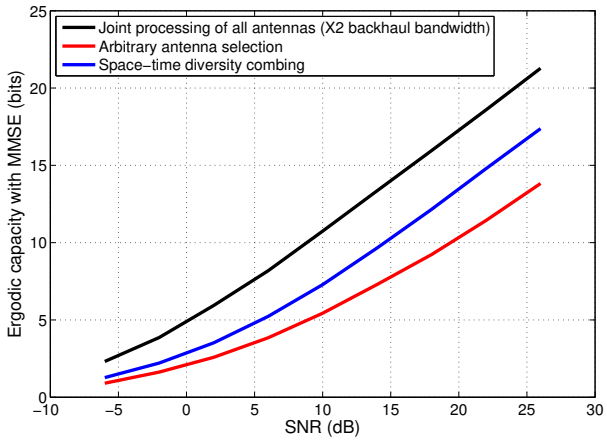

Fig. 10. Comparison of the ergodic capacity of compress-and-forward coupled with linear MMSE equalization and decoding in the cloud, for the three considered combining methods.

Attempting to apply orthogonal designs, one immediately confronts a basic obstacle due to the fact that rate 1 complex orthogonal designs do not exist beyond the case of two antennas. We next demonstrate the problem that arises and also show how it may be resolved by judiciously combining balanced rate $1/2$ orthogonal designs [14] (which includes the four basic OSTBCs described in [15] for 2-8 antennas) with repeated quantization used in conjunction with multiplicative dithering. For the sake of concreteness and ease of exposition, we demonstrate the method for the case of four receive antennas.

The received signals are given by (1) where now $i = 1, \ldots, M$ (with $M = 4$). We proceed by stacking $T = 8$ time instances of the received signal from the 4 antennas and build an effective real-valued vector by decomposing each entry into its real and imaginary components, just as is done in (2). This yields for $M = 4$, a vector $\mathbf{s}$ of dimension $2 \times 4 \times 8 = 64$.

By reinterpreting the rate $1/2$ orthogonal design of 4 trans-

mit antennas (see [15]), we arrive at a 8×64 transformation matrix P as displayed in (26).

$$\mathbf{P} = \begin{bmatrix}
1 & 0 & 0 & 0 & 0 & 0 & 0 & 0 \\
0 & 1 & 0 & 0 & 0 & 0 & 0 & 0 \\
0 & 0 & 1 & 0 & 0 & 0 & 0 & 0 \\
0 & 0 & 0 & 1 & 0 & 0 & 0 & 0 \\
0 & 0 & 0 & 0 & 1 & 0 & 0 & 0 \\
0 & 0 & 0 & 0 & 0 & 1 & 0 & 0 \\
0 & 0 & 0 & 0 & 0 & 0 & 1 & 0 \\
0 & 0 & 0 & 0 & 0 & 0 & 0 & 1 \\
0 & 0 & -1 & 0 & 0 & 0 & 0 & 0 \\
0 & 0 & 0 & -1 & 0 & 0 & 0 & 0 \\
1 & 0 & 0 & 0 & 0 & 0 & 0 & 0 \\
0 & 1 & 0 & 0 & 0 & 0 & 0 & 0 \\
0 & 0 & 0 & 0 & 0 & 0 & -1 & 0 \\
0 & 0 & 0 & 0 & 0 & 0 & 0 & -1 \\
0 & 0 & 0 & 0 & 1 & 0 & 0 & 0 \\
0 & 0 & 0 & 0 & 0 & 1 & 0 & 0 \\
0 & 0 & 0 & 0 & -1 & 0 & 0 & 0 \\
0 & 0 & 0 & 0 & 0 & -1 & 0 & 0 \\
0 & 0 & 0 & 0 & 0 & 0 & 1 & 0 \\
0 & 0 & 0 & 0 & 0 & 0 & 0 & 1 \\
1 & 0 & 0 & 0 & 0 & 0 & 0 & 0 \\
0 & 1 & 0 & 0 & 0 & 0 & 0 & 0 \\
0 & 0 & -1 & 0 & 0 & 0 & 0 & 0 \\
0 & 0 & 0 & -1 & 0 & 0 & 0 & 0 \\
0 & 0 & 0 & 0 & 0 & 0 & -1 & 0 \\
0 & 0 & 0 & 0 & 0 & 0 & 0 & -1 \\
0 & 0 & 0 & 0 & -1 & 0 & 0 & 0 \\
0 & 0 & 0 & 0 & 0 & -1 & 0 & 0 \\
0 & 0 & 1 & 0 & 0 & 0 & 0 & 0 \\
0 & 0 & 0 & 1 & 0 & 0 & 0 & 0 \\
1 & 0 & 0 & 0 & 0 & 0 & 0 & 0 \\
0 & 1 & 0 & 0 & 0 & 0 & 0 & 0 \\
1 & 0 & 0 & 0 & 0 & 0 & 0 & 0 \\
0 & -1 & 0 & 0 & 0 & 0 & 0 & 0 \\
0 & 0 & 1 & 0 & 0 & 0 & 0 & 0 \\
0 & 0 & 0 & -1 & 0 & 0 & 0 & 0 \\
0 & 0 & 0 & 0 & 1 & 0 & 0 & 0 \\
0 & 0 & 0 & 0 & 0 & -1 & 0 & 0 \\
0 & 0 & 0 & 0 & 0 & 0 & 1 & 0 \\
0 & 0 & 0 & 0 & 0 & 0 & 0 & -1 \\
0 & 0 & -1 & 0 & 0 & 0 & 0 & 0 \\
0 & 0 & 0 & 1 & 0 & 0 & 0 & 0 \\
1 & 0 & 0 & 0 & 0 & 0 & 0 & 0 \\
0 & -1 & 0 & 0 & 0 & 0 & 0 & 0 \\
0 & 0 & 0 & 0 & 0 & 0 & -1 & 0 \\
0 & 0 & 0 & 0 & 0 & 0 & 0 & 1 \\
0 & 0 & 0 & 0 & 1 & 0 & 0 & 0 \\
0 & 0 & 0 & 0 & 0 & -1 & 0 & 0 \\
0 & 0 & 0 & 0 & -1 & 0 & 0 & 0 \\
0 & 0 & 0 & 0 & 0 & 1 & 0 & 0 \\
0 & 0 & 0 & 0 & 0 & 0 & 1 & 0 \\
0 & 0 & 0 & 0 & 0 & 0 & 0 & -1 \\
1 & 0 & 0 & 0 & 0 & 0 & 0 & 0 \\
0 & -1 & 0 & 0 & 0 & 0 & 0 & 0 \\
0 & 0 & -1 & 0 & 0 & 0 & 0 & 0 \\
0 & 0 & 0 & 1 & 0 & 0 & 0 & 0 \\
0 & 0 & 0 & 0 & 0 & 0 & -1 & 0 \\
0 & 0 & 0 & 0 & 0 & 0 & 0 & 1 \\
0 & 0 & 0 & 0 & -1 & 0 & 0 & 0 \\
0 & 0 & 0 & 0 & 0 & 1 & 0 & 0 \\
0 & 0 & 1 & 0 & 0 & 0 & 0 & 0 \\
0 & 0 & 0 & -1 & 0 & 0 & 0 & 0 \\
1 & 0 & 0 & 0 & 0 & 0 & 0 & 0 \\
0 & -1 & 0 & 0 & 0 & 0 & 0 & 0
\end{bmatrix}^T \tag{26}$$

Next, we form a 8×1 real vector $\mathbf{u}$ by applying to the effective received vector $\mathbf{s}$, formed in the manner described in (2), the transformation

$$\mathbf{u} = \frac{1}{\sqrt{8}} P\mathbf{s}$$

It can be shown that the following holds

$$\begin{aligned}
\mathbf{u} &= \frac{1}{\sqrt{8}} U(h_1, h_2, h_3, h_4)\mathbf{x} + P\mathbf{n} \\
&= \frac{1}{\sqrt{8}} U(h_1, h_2, h_3, h_4)\mathbf{x} + \mathbf{n}'
\end{aligned} \tag{27}$$

where $U(h_1, h_2, h_3, h_4)$ is displayed in (28). Here, the vector $\mathbf{x}$ is the 16-dimensional real representation of the transmitted signal over $T = 8$ time instances, formed analogously to (3).

$$\mathbf{U}(h_1, h_2, h_3, h_4) = \begin{bmatrix}
h_{1R} & h_{1I} & h_{2R} & h_{2I} & h_{3R} & h_{3I} & h_{4R} & h_{4I} \\
-h_{1I} & h_{1R} & -h_{2I} & h_{2R} & -h_{3I} & h_{3R} & -h_{4I} & h_{4R} \\
h_{2R} & h_{2I} & -h_{1R} & -h_{1I} & h_{4R} & h_{4I} & -h_{3R} & -h_{3I} \\
-h_{2I} & h_{2R} & h_{1I} & -h_{1R} & -h_{4I} & h_{4R} & h_{3I} & -h_{3R} \\
h_{3R} & h_{3I} & -h_{4R} & -h_{4I} & -h_{1R} & -h_{1I} & h_{2R} & h_{2I} \\
-h_{3I} & h_{3R} & h_{4I} & -h_{4R} & h_{1I} & -h_{1R} & -h_{2I} & h_{2R} \\
h_{4R} & h_{4I} & h_{3R} & h_{3I} & -h_{2R} & -h_{2I} & -h_{1R} & -h_{1I} \\
-h_{4I} & h_{4R} & -h_{3I} & h_{3R} & h_{2I} & -h_{2R} & h_{1I} & -h_{1R} \\
h_{1R} & -h_{1I} & h_{2R} & -h_{2I} & h_{3R} & -h_{3I} & h_{4R} & -h_{4I} \\
-h_{1I} & -h_{1R} & -h_{2I} & -h_{2R} & -h_{3I} & -h_{3R} & -h_{4I} & -h_{4R} \\
h_{2R} & -h_{2I} & -h_{1R} & h_{1I} & h_{4R} & -h_{4I} & -h_{3R} & h_{3I} \\
-h_{2I} & -h_{2R} & h_{1I} & h_{1R} & -h_{4I} & -h_{4R} & h_{3I} & h_{3R} \\
h_{3R} & -h_{3I} & -h_{4R} & h_{4I} & -h_{1R} & h_{1I} & h_{2R} & -h_{2I} \\
-h_{3I} & -h_{3R} & h_{4I} & h_{4R} & h_{1I} & h_{1R} & -h_{2I} & -h_{2R} \\
h_{4R} & -h_{4I} & h_{3R} & -h_{3I} & -h_{2R} & h_{2I} & -h_{1R} & h_{1I} \\
-h_{4I} & -h_{4R} & -h_{3I} & -h_{3R} & h_{2I} & h_{2R} & h_{1I} & h_{1R}
\end{bmatrix}^T \tag{28}$$

We note that rows of $U(h_1, h_2, h_3, h_4)$ are orthogonal for any values of $h_1, \ldots, h_4$. From this, it also follows that $\mathbf{n}'$ is white (and Gaussian with unit variance).

The problem with using a non-rate 1 orthogonal design now becomes clear. Unlike $U(h_1, h_2)$ (see (6)) which is square, $U(h_1, h_2, h_3, h_4)$ on the other hand is non-square and hence is non-invertible.

We overcome this obstacle by passing the same observation vector $\mathbf{s}$ via a "dithered" version of P, such that another set of 8 mutually orthogonal measurement rows is attained.

Specifically, let us define a 4 dimensional vector $d = (d_1, d_2, d_3, d_4)$ where d_i are complex numbers of unit magnitude (pure phases). We form a dithered version of the antenna outputs as

$$\tilde{s}_i(t) = d_i \cdot s_i(t), \tag{29}$$

where d_i does not depend on t. We assume that the d_i are drawn at random as i.i.d. uniform phases.

We may associate with $\tilde{s}_i(t)$, $t = 1, \ldots, T = 8$, the effective 64-dimensional real vector $\tilde{\mathbf{s}}$. Next, we obtain another 8-dimensional real vector $\tilde{\mathbf{u}}$ by applying to the vector $\tilde{\mathbf{s}}$ the transformation

$$\tilde{\mathbf{u}} = \frac{1}{\sqrt{8}} P\tilde{\mathbf{s}} \tag{30}$$

We therefore obtain

$$\tilde{\mathbf{u}} = \frac{1}{\sqrt{8}} U(d_1 h_1, d_2 h_2, d_3 h_3, d_4 h_4)\mathbf{x} + \mathbf{n}'' \tag{31}$$

where $\mathbf{n}''$ is distributed as $\mathbf{n}'$ (and of course is a function of it).

Note that the dithers drawn implicitly (via (29) and (30)) define a

"dithered" combining matrix $\tilde{P}$. Combining (27) and (31), we have

$$\underbrace{\begin{bmatrix} \mathbf{u} \\ \tilde{\mathbf{u}} \end{bmatrix}}_{\mathbf{u}_{\text{eff}}} = \underbrace{\begin{bmatrix} U(h_1,h_2,h_3,h_4) \\ U(d_1h_1,d_2h_2,d_3h_3,d_4h_4) \end{bmatrix}}_{\mathcal{F}} \mathbf{x} + \begin{bmatrix} \mathbf{n}' \\ \mathbf{n}'' \end{bmatrix} \tag{32}$$

Finally, we apply component-wise quantization to obtain

$$\mathbf{y} = Q(\mathbf{u}_{\text{eff}}). \tag{33}$$

We may then recover an estimate of $\mathbf{x}$ by applying the inverse of $\mathcal{F}$ to $\mathbf{y}$ or a linear MMSE estimator.

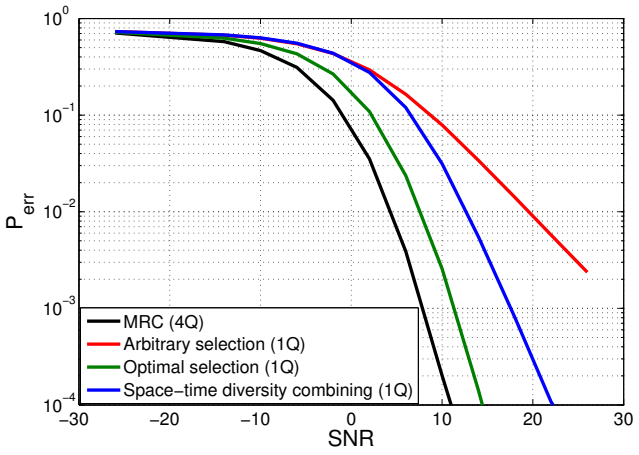

Fig. 11. Performance of bit error rate of new space-time diversity scheme and comparison with alternatives.

REFERENCES

[1] D. G. Brennan, "Linear diversity combining techniques," *Proceedings of the IRE*, vol. 47, no. 6, pp. 1075–1102, 1959.

[2] S. Sanayei and A. Nosratinia, "Antenna selection in MIMO systems," *IEEE Communications Magazine*, vol. 42, no. 10, pp. 68–73, 2004.

[3] A. F. Molisch and M. Z. Win, "MIMO systems with antenna selection," *IEEE microwave magazine*, vol. 5, no. 1, pp. 46–56, 2004.

[4] N. Mangalvedhe, R. Ratasuk, and A. Ghosh, "NB-IoT deployment study for low power wide area cellular IoT," in *Personal, Indoor, and Mobile Radio Communications (PIMRC), 2016 IEEE 27th Annual International Symposium on*. IEEE, 2016, pp. 1–6.

[5] Y.-P. E. Wang, X. Lin, A. Adhikary, A. Grovlen, Y. Sui, Y. Blankenship, J. Bergman, and H. S. Razaghi, "A primer on 3GPP narrowband internet of things," *IEEE Communications Magazine*, vol. 55, no. 3, pp. 117–123, 2017.

[6] M. R. Palattella, M. Dohler, A. Grieco, G. Rizzo, J. Torsner, T. Engel, and L. Ladid, "Internet of things in the 5G era: Enablers, architecture, and business models," *IEEE Journal on Selected Areas in Communications*, vol. 34, no. 3, pp. 510–527, 2016.

[7] P. Rost, C. J. Bernardos, A. De Domenico, M. Di Girolamo, M. Lalam, A. Maeder, D. Sabella, and D. Wübben, "Cloud technologies for flexible 5G radio access networks," *IEEE Communications Magazine*, vol. 52, no. 5, pp. 68–76, 2014.

[8] D. Wubben, P. Rost, J. S. Bartelt, M. Lalam, V. Savin, M. Gorgoglione, A. Dekorsy, and G. Fettweis, "Benefits and impact of cloud computing on 5G signal processing: Flexible centralization through cloud-ran," *IEEE signal processing magazine*, vol. 31, no. 6, pp. 35–44, 2014.

[9] F. Boccardi, R. W. Heath, A. Lozano, T. L. Marzetta, and P. Popovski, "Five disruptive technology directions for 5G," *IEEE Communications Magazine*, vol. 52, no. 2, pp. 74–80, 2014.

[10] S.-H. Park, O. Simeone, O. Sahin, and S. S. Shitz, "Fronthaul compression for cloud radio access networks: Signal processing advances inspired by network information theory," *IEEE Signal Processing Magazine*, vol. 31, no. 6, pp. 69–79, 2014.

[11] O. Tirkkonen, A. Boariu, and A. Hottinen, "Minimal non-orthogonality rate 1 space-time block code for 3+ tx antennas," in *Spread Spectrum Techniques and Applications, 2000 IEEE Sixth International Symposium on*, vol. 2. IEEE, 2000, pp. 429–432.

[12] H. Jafarkhani, "A quasi-orthogonal space-time block code," *IEEE Transactions on Communications*, vol. 49, no. 1, pp. 1–4, 2001.

[13] N. Sharma and C. B. Papadias, "Improved quasi-orthogonal codes through constellation rotation," *IEEE Transactions on Communications*, vol. 51, no. 3, pp. 332–335, 2003.

[14] S. S. Adams, J. Davis, N. Karst, M. K. Murugan, B. Lee, M. Crawford, and C. Greeley, "Novel classes of minimal delay and low PAPR rate 1/2 complex orthogonal designs," *IEEE Transactions on Information Theory*, vol. 57, no. 4, pp. 2254–2262, 2011.

[15] V. Tarokh, H. Jafarkhani, and A. R. Calderbank, "Space-time block codes from orthogonal designs," *IEEE Transactions on Information theory*, vol. 45, no. 5, pp. 1456–1467, 1999.